MM-131, a bispecific anti-Met/EpCAM mAb, inhibits HGF-dependent and HGF-independent Met signaling through concurrent binding to EpCAM

Jessica B. Casaletto, Melissa L. Geddie, Adnan O. Abu-Yousif, Kristina Masson, Aaron Fulgham, Antoine Boudot, Tim Maiwald, Jeffrey D. Kearns, Neeraj Kohli, Stephen Su, Maja Razlog, Andreas Raue, Ashish Kalra, Maria Håkansson, Derek T. Logan, Martin Welin, Shrikanta Chattopadhyay, Brian D. Harms, Ulrik B. Nielsen, Birgit Schoeberl, Alexey A. Lugovskoy, Gavin MacBeath

Angaben zur Veröffentlichung / Publication details:

Casaletto, Jessica B., Melissa L. Geddie, Adnan O. Abu-Yousif, Kristina Masson, Aaron Fulgham, Antoine Boudot, Tim Maiwald, et al. 2019. "MM-131, a bispecific anti-Met/EpCAM mAb, inhibits HGF-dependent and HGF-independent Met signaling through concurrent binding to EpCAM." *PNAS* 116 (15): 7533–42. https://doi.org/10.1073/pnas.1819085116.

MM-131, a bispecific anti-Met/EpCAM mAb, inhibits HGF-dependent and HGF-independent Met signaling through concurrent binding to EpCAM

Jessica B. Casaletto[a], Melissa L. Geddie[a], Adnan O. Abu-Yousif[a], Kristina Masson[a], Aaron Fulgham[a], Antoine Boudot[a], Tim Maiwald[a], Jeffrey D. Kearns[a], Neeraj Kohli[a], Stephen Su[a], Maja Razlog[a], Andreas Raue[a,1], Ashish Kalra[a], Maria Håkansson[b], Derek T. Logan[b], Martin Welin[b], Shrikanta Chattopadhyay[a], Brian D. Harms[a], Ulrik B. Nielsen[a], Birgit Schoeberl[a], Alexey A. Lugovskoy[a], and Gavin MacBeath[a,1]

[a]Discovery Division, Merrimack Pharmaceuticals, Inc., Cambridge, MA 02139; and [b]SARomics Biostructures AB, Medicon Village, SE-223 81 Lund, Sweden

Activation of the Met receptor tyrosine kinase, either by its ligand, hepatocyte growth factor (HGF), or via ligand-independent mechanisms, such as *MET* amplification or receptor overexpression, has been implicated in driving tumor proliferation, metastasis, and resistance to therapy. Clinical development of Met-targeted antibodies has been challenging, however, as bivalent antibodies exhibit agonistic properties, whereas monovalent antibodies lack potency and the capacity to down-regulate Met. Through computational modeling, we found that the potency of a monovalent antibody targeting Met could be dramatically improved by introducing a second binding site that recognizes an unrelated, highly expressed antigen on the tumor cell surface. Guided by this prediction, we engineered MM-131, a bispecific antibody that is monovalent for both Met and epithelial cell adhesion molecule (EpCAM). MM-131 is a purely antagonistic antibody that blocks ligand-dependent and ligand-independent Met signaling by inhibiting HGF binding to Met and inducing receptor down-regulation. Together, these mechanisms lead to inhibition of proliferation in Met-driven cancer cells, inhibition of HGF-mediated cancer cell migration, and inhibition of tumor growth in HGF-dependent and -independent mouse xenograft models. Consistent with its design, MM-131 is more potent in EpCAM-high cells than in EpCAM-low cells, and its potency decreases when EpCAM levels are reduced by RNAi. Evaluation of Met, EpCAM, and HGF levels in human tumor samples reveals that EpCAM is expressed at high levels in a wide range of Met-positive tumor types, suggesting a broad opportunity for clinical development of MM-131.

bispecific antibody | Met | HGF | EpCAM | cancer

Signaling by the Met receptor tyrosine kinase promotes proliferation, migration, and survival, which, in turn, underlie the processes of developmental morphogenesis, wound repair, and organ homeostasis (1, 2). Dysregulation of Met signaling is linked to cancer progression, metastasis, and resistance to therapy. Aberrant Met activation has been reported in many cancers and can occur via ligand-dependent and ligand-independent mechanisms. The only known Met ligand, hepatocyte growth factor (HGF), can be produced locally through autocrine and/or paracrine mechanisms. For example, tumors of mesenchymal origin often produce their own HGF, whereas tumor-associated fibroblasts can produce HGF to promote tumor progression in a paracrine manner (3–5). In addition to HGF-induced Met activation, ligand-independent signaling can occur via *MET* gene amplification or mutation, receptor overexpression resulting from transcriptional up-regulation, or transactivation by other membrane receptors (2, 6, 7). Elevated levels of Met and/or HGF can confer resistance to therapy, including chemotherapy, radiotherapy, and targeted therapies such as EGF receptor (EGFR) inhibitors (8–10). Moreover, high HGF and Met levels are associated with poor clinical outcomes, including increased metastasis and decreased survival (11–14).

Given the roles of the Met signaling pathway in tumor progression and its negative impact on clinical outcomes, Met is a therapeutic target that remains under intense investigation. Optimal targeting of the pathway, however, requires an agent that is effective in blocking both HGF-dependent and HGF-independent signaling. Although small-molecule tyrosine kinase inhibitors (TKIs) designed to inhibit Met activity can, in principle, achieve this, first-generation Met TKIs suffer from a lack of selectivity (15). Recent clinical studies with more selective Met TKIs have reported encouraging response rates in patients with *MET*-amplified tumors (16–18). Unfortunately, patients have typically progressed relatively rapidly on Met TKIs, with an average progression-free survival (PFS) of 3.5 mo (19, 20). Notably, both innate and acquired resistance to TKIs has been attributed to tumor microenvironment-derived production of HGF (21). As

Significance

Although *MET* is an established oncogene that drives tumorigenesis, metastasis, and resistance to therapy, antibody therapeutics targeting Met have thus far eluded successful clinical development. Met is a particularly challenging target because bivalent antibodies typically agonize Met, whereas monovalent antibodies lack potency and the capacity to downregulate it. We report the design and preclinical development of a purely antagonistic anti-Met antibody that potently blocks both ligand-dependent and ligand-independent signaling by exploiting the concept of avidity. MM-131 is a bispecific antibody that is monovalent for Met, but exhibits high avidity by concurrently binding to the tumor-specific antigen epithelial cell adhesion molecule. Preclinically, MM-131 inhibits proliferation in Met-driven cancer cells, inhibits hepatocyte growth factor (HGF)-mediated cell migration, and inhibits tumor growth in HGF-dependent and -independent mouse xenograft models.

Author contributions: J.B.C., M.L.G., A.O.A.-Y., K.M., A.R., B.D.H., U.B.N., B.S., A.A.L., and G.M. designed research; J.B.C., M.L.G., A.O.A.-Y., K.M., A.F., A.B., T.M., J.D.K., N.K., S.S., M.R., A.K., M.H., D.T.L., and M.W. performed research; J.B.C., M.L.G., A.O.A.-Y., K.M., A.F., A.B., T.M., J.D.K., N.K., S.S., M.R., A.K., M.H., D.T.L., M.W., S.C., and B.D.H. analyzed data; and J.B.C., M.L.G., T.M., J.D.K., A.R., M.H., and G.M. wrote the paper.

Conflict of interest statement: Several authors are or were employees of Merrimack Pharmaceuticals, Inc. at the time of contributing to the manuscript.

Data deposition: The atomic coordinates and structure factors have been deposited in the Protein Data Bank, www.wwpdb.org (PDB ID codes 6HYG, for the Fc domain; 6I07, for the scFV::EpCAM complex; and 6I04, for the Fab::Met complex). Data and code for the computational model are available at http://www.data2dynamics.org/.

[1]To whom correspondence may be addressed. Email: araue@merrimack.com or gavin.macbeath@gmail.com.

This article contains supporting information online at www.pnas.org/lookup/suppl/doi:10.1073/pnas.1819085116/-/DCSupplemental.

an alternative strategy, development of therapeutic HGF/Met-blocking antibodies has also been pursued. Generation of antibodies effective in blocking both ligand-dependent and ligand-independent Met signaling has been difficult, however, as monovalent antibodies lack potency, whereas bivalent antibodies often promote receptor dimerization and activation (22, 23). To overcome these challenges, bispecific antibodies have been proposed (24, 25). Here, we engineered MM-131, a bispecific antibody that is monovalent for Met, but has increased potency by concurrently binding the tumor surface antigen, epithelial cell adhesion molecule (EpCAM). EpCAM is a transmembrane glycoprotein, originally discovered on colon carcinomas, that is highly expressed in most cancers of epithelial origin, but is expressed at much lower levels in normal epithelia and is spatially restricted to tight junctions (26–28).

Here, we demonstrate that MM-131 is a purely antagonistic antibody that blocks both HGF-dependent and HGF-independent Met signaling in EpCAM-positive cells by inhibiting HGF binding to Met and downregulating Met receptor levels. These two mechanisms lead to the inhibition of Met-driven cancer cell proliferation and migration in vitro and the inhibition of HGF-dependent and -independent tumor growth in vivo. Evaluation of Met, HGF, and EpCAM levels in human tumor samples reveals that EpCAM is expressed at high levels in a wide range of Met-positive tumor types, highlighting the potential for broad clinical development of MM-131.

Results

Design of MM-131. Previous studies have shown that standard, bivalent antibodies targeting Met are potent antagonists in the presence of HGF, but often have the unintended and undesired effect of activating Met in the absence of ligand. One way to circumvent this problem is to engineer monovalent anti-Met antibodies (MetMAbs), such as onartuzumab (huOA-5D5) (29). Although this strategy reduces or eliminates antibody-induced Met activation, it renders the agent substantially less potent (higher EC_{50}) than the corresponding bivalent antibody and unable to induce receptor down-regulation. One way to increase potency is to exploit the concept of avidity. The functional affinity of a monovalent antibody can, in principle, be increased simply by raising its local concentration at the cell surface through concurrent binding to another unrelated cell surface antigen. Guided by this principle, we designed MM-131 as a bispecific molecule that targets Met and the tumor antigen, EpCAM (Fig. 1*A*). The engineering aspects of the bispecific format are discussed in the next section. EpCAM is not intended as a therapeutic target of MM-131, but is instead used as an "anchor" to preconcentrate MM-131 at the cell surface (EpCAM is usually present at much higher levels than Met). Previously, Harms et al. (30) described a computational framework for designing and optimizing bispecific antibodies to ensure efficient cross-arm binding, given the relative expression of each target. Using this model, MM-131 was designed to have high affinity for Met (K_d = 0.2 nM) and moderate affinity for EpCAM (K_d = 10 nM). A computational simulation using these parameters, with 10^5 Met receptors per cell and 10^6 EpCAM receptors per cell, demonstrates the theoretic effect of EpCAM targeting on binding avidity (Fig. 1*B*).

Engineering and Structure of MM-131. Overall, MM-131 comprises three components: (*i*) a monovalent, human anti-Met Fab that binds to the Sema domain of human Met; (*ii*) a stability-engineered IgG1/IgG4 backbone; and (*iii*) a single-chain antibody fragment (scFv) that targets EpCAM (Fig. 1*A*). To generate a bispecific antibody, MM-131 was engineered with an asymmetrical Fc region by introducing knob-into-hole mutations (31), rendering it heterodimeric. Size exclusion chromatography (SEC) analysis revealed, however, that the resulting protein was only 50% correctly assembled and nonaggregated (*SI Appendix*, Fig. S1*A*, sample 1). To improve antibody homogeneity, we tested different antibody isotypes for the Fc region (IgG1, IgG4, and a hybrid generated by combining the IgG4 CH2 domain with the IgG1 CH3 domain), as well as different hinge sequences (IgG1, IgG4) and the addition of a flexible linker between the Fc regions. Analysis of the resulting variants using SEC (*SI Appendix*, Fig. S1*A*) and SDS/PAGE (*SI Appendix*, Fig. S1*B*) showed that the fully IgG1 variant and the IgG4/IgG1 chimera were each ∼80% nonaggregated. To further increase antibody homogeneity and stability, we investigated additional changes, including using an alternative knob-into-hole mutation (Y407T/T366Y), adding disulfide bonds, and changing the Fc linker length. The resulting antibody variants ranged from ∼55% to ∼90% nonaggregated (*SI Appendix*, Fig. S1*C*). Interestingly, the most improved variants from each isotype had different mutations. The best IgG1/IgG4 variant (∼90% nonaggregated) contained an additional disulfide bond near the C terminus of CH3 and a 40-aa linker, whereas the best IgG1 variant (∼90% nonaggregated) contained no additional disulfide bonds and a 20-aa linker. Stability assays performed with these two molecules, including freeze/thaw cycles, agitation, and elevated temperature, showed that the IgG1/IgG4 hybrid was more stable and slightly more nonaggregated (*SI Appendix*, Fig. S1*D*). Finally, we optimized the deglycosylation site using complementary charge pairing to further enhance stability (*SI Appendix*, Table S1).

To ensure that the modifications used to generate a stable, homogeneous Fc backbone did not substantially affect antibody structure, we purified and crystallized the Fc region of MM-131 (Fig. 1*C*). The structure was determined to 2.3 Å resolution by molecular replacement, with the IgG4 Fc having Protein Data Bank (PDB) ID code 3C2S (32) as the search model. The crystallographic data are provided in *SI Appendix*, Table S2. Overall, MM-131 Fc is more similar to a glycosylated IgG4 CH2 (rmsd = 0.94 Å for 406 of 416 residues compared with PDB ID code 4C54) (33, 34) than to an aglycosylated IgG4 CH2 (rmsd = 1.76 Å for 406 of 416 residues compared with PDB ID code 4D2N) (35) (Fig. 1*D*). This is consistent with the intended role of the complementary charge pair introduced at position 299 of the CH2 domains, which acts to restabilize the domain following deglycosylation. As the CH3 region of MM-131 contains knob-into-hole mutations, we compared the CH3 region of MM-131 with a previously published knob-into-hole structure. As anticipated, the CH3 region of MM-131 aligned well (rmsd = 1.59 Å for 413 of 416 residues compared with PDB ID code 4NQS) (36), confirming that our design did not result in any unanticipated structural perturbations.

To choose an anti-Met Fab, a panel of fully human anti-Met antibodies was generated using a yeast-based antibody display platform (Adimab LLC) and binned by epitope. Antibodies in both IgG and Fab formats were assayed for activation of Met in the absence of HGF. In the bivalent IgG format, all anti-Met antibodies induced phosphorylation of Met, although the degree of agonism was epitope-dependent, with epitope bin 3 demonstrating the least agonistic activity (*SI Appendix*, Fig. S2*A*). In contrast, the corresponding Fabs, which are monovalent for Met, showed no agonistic activity (*SI Appendix*, Fig. S2*B*). Using these data, we selected as the anti-Met portion of MM-131 a Fab from epitope bin 3 that demonstrated low aggregation properties, high thermal stability, and high expression yields in CHO cells. To identify the epitope on Met that this portion recognizes, we purified and crystallized a complex containing the anti-Met Fab of MM-131, along with the Sema domain of Met. The structure was solved to 3.1 Å resolution, and the structure was solved by molecular replacement using PDB ID code 4PY7 (37) as a search model for the Fab and PDB ID code 4O3T (38) for Met. The structure of the Met Sema domain was nearly identical to previously reported structures of Met, with an rmsd (33) from Met in PDB ID code 4O3T of 0.71 Å for 432 atoms compared. Further, the crystal structure revealed that the anti-Met Fab of MM-131 binds to propeller blades 2 and 3 of the Met Sema domain, with residues from all six complementarity-determining regions

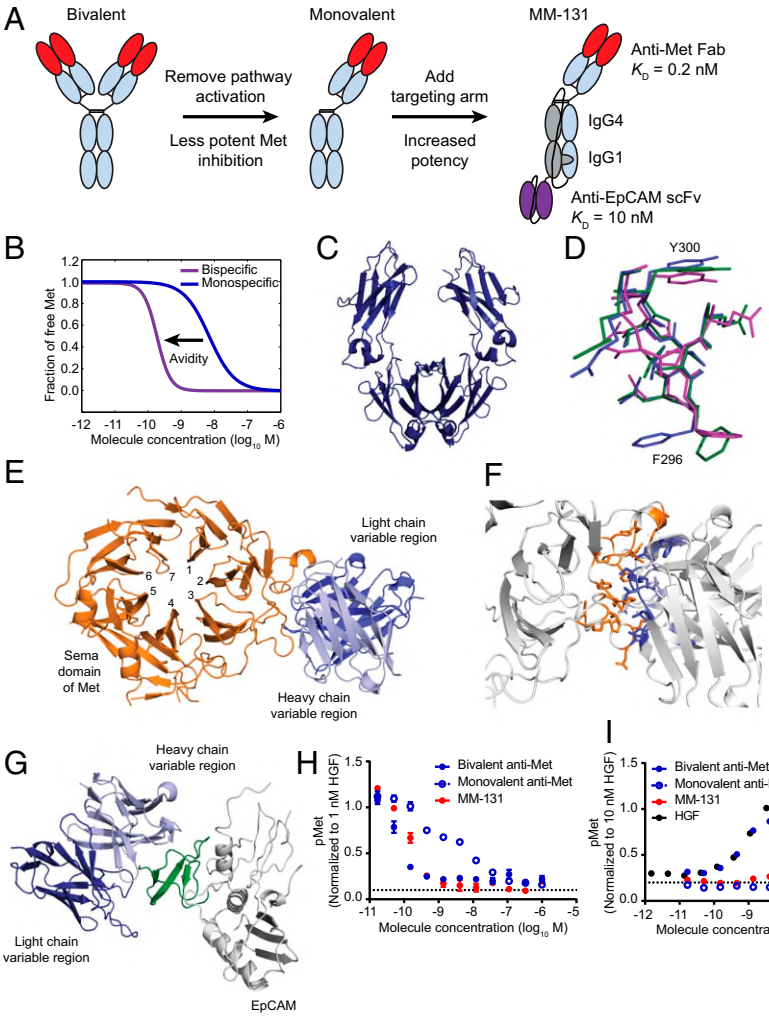

Fig. 1. Design of a bispecific anti-Met antibody cotargeting EpCAM (MM-131). (*A*) Schematic of the design of MM-131. To ensure monovalency for Met, the Fc region was engineered to include "knob-into-hole" mutations, a C-terminal disulfide bond, and a linker connecting the Fc regions. (*B*) Simulation of Met inhibition by a monovalent, monospecific antibody without a targeting arm (K_d = 0.2 nM) and the increased avidity afforded by inclusion of an EpCAM targeting arm (K_d = 10 nM). Simulations were performed assuming Met expression of 10^5 receptors per cell and EpCAM expression of 10^6 receptors per cell. (*C*) Ribbon diagram of the Fc region of MM-131. (*D*) DE loop of the Fc domain of MM-131 (green), overlaid with the glycosylated IgG4 CH2 domain of PDB ID code 4C54 (purple) and the aglycosylated IgG4 CH2 domain of PDB ID code 4D2N (blue). (*E*) Ribbon diagram of the anti-Met Fab of MM-131 (blue), cocrystallized with the Sema domain of Met (orange). (*F*) Close-up view of the interface between MM-131 (blue) and the Sema domain of Met (orange). (*G*) Ribbon diagram of the anti-EpCAM scFv of MM-131 (blue), cocrystallized with the extracellular domain of EpCAM (gray). The N-terminal domain of EpCAM (pyroGlu24-Leu62) is highlighted in green. (*H*) MM-131 potently inhibits HGF-mediated phosphorylation of Met. MM-131 was compared with monovalent anti-Met Fab and with bivalent anti-Met IgG, both based on the anti-Met–binding domain of MM-131. Antibodies were incubated with HT-29 cells for 2 h before 10 min of stimulation with 1 nM HGF. Lysates were analyzed by pMet ELISA; the dotted line indicates the pMet level in the absence of HGF and antibodies (media control). (*I*) Similar to monovalent anti-Met Fab, MM-131 does not activate Met signaling. HT-29 cells were incubated with HGF, MM-131, bivalent anti-Met, monovalent anti-Met, or media for 10 min. Lysates were analyzed by pMet ELISA; the dotted lines indicate the pMet level of cells in media alone. Plots in *H* and *I* reflect mean (n = 4) and SEM.

(CDRs) involved in binding (Fig. 1*E*). The antibody/antigen interface has a buried surface area of 1,200 Å^2 (39) and includes hydrogen bonds and a salt bridge (Fig. 1*F*). The epitope of Met that is recognized by MM-131 is in a similar region to that recognized by LY2875358 (the bivalent anti-Met antibody previously developed by Eli Lilly) (40). However, it differs substantially from the epitope recognized by onartuzumab, which spans propeller blades 4, 5, and 6 of the Sema domain (29). The epitope recognized by the anti-Met Fab of MM-131 overlaps with the HGF-β–binding site of Met (41), suggesting that MM-131 blocks binding of HGF-β to Met (as reported for LY2875358) (40).

Moc31 is a well-characterized anti-EpCAM antibody (42) that is amenable to humanization and stabilization (43). We stabilized moc31 onto different antibody frameworks, tested different orientations of the VH-VL domains, and screened for developability, including the percentage monomer after initial purification (*SI Appendix*, Fig. S3). In addition, we removed a potential site of deamidation on CDR-L1 to improve homogeneity of the scFv. This change reduced the affinity of the resulting scFv, shifting its equilibrium K_d from ∼3 nM to 10 nM. To determine the epitope on EpCAM recognized by this scFv, we purified and crystallized the anti-EpCAM scFv complexed with the extracellular domain of EpCAM. The structure was solved to 2.35 Å by molecular replacement using PDB ID codes 1SVZ for the scFv and 4MZV for EpCAM. Overall, the structure of EpCAM in the scFv::EpCAM complex is very similar to a previously published structure of EpCAM (PDB ID code 4MZV) (44), with an rmsd of 1.02 Å for 222 atoms compared (33). As in the previously published structure, EpCAM contains a pyroglutamate at its N terminus, rather than a glutamine. The asymmetrical unit comprises an EpCAM dimer to which two monomeric scFvs are bound. The conformation of the dimer is *in cis*, which has previously been shown to be important for EpCAM activity (44). Previous domain mapping has shown that most anti-EpCAM antibodies recognize the N-terminal domain of EpCAM (45). Consistent with this, the epitope for the anti-EpCAM scFv is in the N-terminal domain (pyroGlu24-Leu62) (Fig. 1*G*). The interface between the loops of the antibody and EpCAM is relatively small, with a buried surface area of 878 Å^2 (39).

When engineering an antibody for therapeutic use, it is important to optimize the biological activity of the antibody as well as to ensure it has the appropriate biophysical properties to enable large-scale manufacturing and long-term storage. To test the effectiveness of our bispecific antibody design, we compared MM-131 with the related monovalent anti-Met Fab (no EpCAM targeting) and the related bivalent anti-Met IgG (Fig. 1 *H* and *I*). As predicted by the model in Fig. 1*B*, both MM-131 and the bivalent anti-Met IgG potently inhibit HGF-mediated Met phosphorylation, whereas the monovalent anti-Met Fab is substantially less potent (Fig. 1*H*). In the absence of HGF, however, the bivalent anti-Met IgG activates Met signaling, whereas both the monovalent Fab and MM-131 show no discernible agonistic activity (Fig. 1*I*). To assess the stability of MM-131, we developed a purification scheme with resins suitable for large-scale manufacturing,

protein A and hydroxyapatite, resulting in material that was 97.8% monomeric (*SI Appendix*, Fig. S4*A*). After 14 mo at 4 °C, the antibody was 96.2% monomeric, demonstrating its potential for long-term storage (*SI Appendix*, Fig. S4*B*).

EpCAM Targeting Enhances Blockade of Downstream Signaling. To assess the effects of MM-131 on downstream signaling, as well as to determine how different levels of Met and EpCAM affect MM-131 activity, we built a mechanistic model of Met signaling comprising ordinary differential equations. Each equation describes either a protein-binding or catalytic event in the network, and the model includes intracellular signaling pathways and receptor trafficking. Model simulations suggested that MM-131 would provide enhanced inhibition of pAkt relative to the monovalent antibody, huOA-5D5, across a wide range of Met and EpCAM surface receptor levels (Fig. 2*A*). Importantly, most cell lines derived from epithelial cancers fall into an area of this space that strongly favors MM-131 over huOA-5D5 (Fig. 2*A* and *SI Appendix*, Table S3).

Using this model, three cell lines were selected that lie in regions where MM-131 is predicted to show either enhanced (NCI-H747 and NCI-H441) or nearly equivalent (A549) activity relative to huOA-5D5 (Fig. 2*A*). Cells were then incubated with either MM-131 or huOA-5D5, stimulated with 1 nM HGF for 10 min, and analyzed for pAkt (S473) by ELISA (Fig. 2*B* and *SI Appendix*, Fig. S5*A*). MM-131 was more potent than huOA-5D5 in cells with a high EpCAM/Met ratio and equipotent in cells with a low EpCAM/Met ratio. Further validation was carried out in isogenic cell lines in which EpCAM was stably knocked down by RNAi. As predicted, lowering the EpCAM level (and hence the EpCAM/Met ratio) in NCI-H747 and NCI-H441 cells rendered MM-131 less potent at inhibiting HGF-mediated Met pathway activation (Fig. 2*C* and *SI Appendix*, Fig. S5*B* and Table S4).

Dual Mechanism of Action of MM-131. MM-131 contains an anti-Met Fab that binds to propeller blades 2 and 3 of the Met Sema domain, overlapping the HGF-β–binding site. This is similar to the epitope reported for the bivalent anti-Met antibody LY2875358, but dissimilar from that of huOA-5D5, which binds to propeller blades 4, 5, and 6 and is reported to block HGF-α binding (29, 40). In contrast, the bivalent anti-Met antibody ABT-700 binds an epitope outside the Sema domain and is reported to block Met dimerization (46). To confirm that MM-131 is HGF-competitive, biolayer interferometry was used to measure the HGF-blocking properties of MM-131, LY2875358, huOA-5D5, and ABT-700. Antibodies were loaded onto anti-human IgG Fc capture biosensors, followed by sequential incubation with 200 nM human Met, 200 nM human HGF, and PBS. As expected, MM-131, huOA-5D5, and LY2875358 all blocked HGF binding to Met, whereas ABT-700 did not (Fig. 3*A*). By blocking HGF binding to Met, MM-131 prevents HGF-mediated Met phosphorylation and activation of Gab1, Akt, MAPK (Erk1/2), and S6 in a dose-dependent manner (Fig. 3*B*).

In addition to HGF-induced Met activation, Met can be activated by HGF-independent mechanisms, including gene amplification, mutation, and transcriptional up-regulation. To block both HGF-dependent and HGF-independent Met signaling, MM-131 was designed to down-regulate the receptor. Antibody-mediated receptor down-regulation, which occurs via receptor internalization and degradation, typically requires bivalent binding; thus, huOA-5D5 does not induce this effect. In contrast, MM-131 induces down-regulation of Met in both *MET*-amplified (*SI Appendix*, Fig. S6*A*) and nonamplified (Fig. 3*C*) EpCAM-positive cells in the absence of HGF. The magnitude of this effect depends on the bivalent binding of MM-131 to EpCAM; less effective down-regulation of Met was observed using a version of

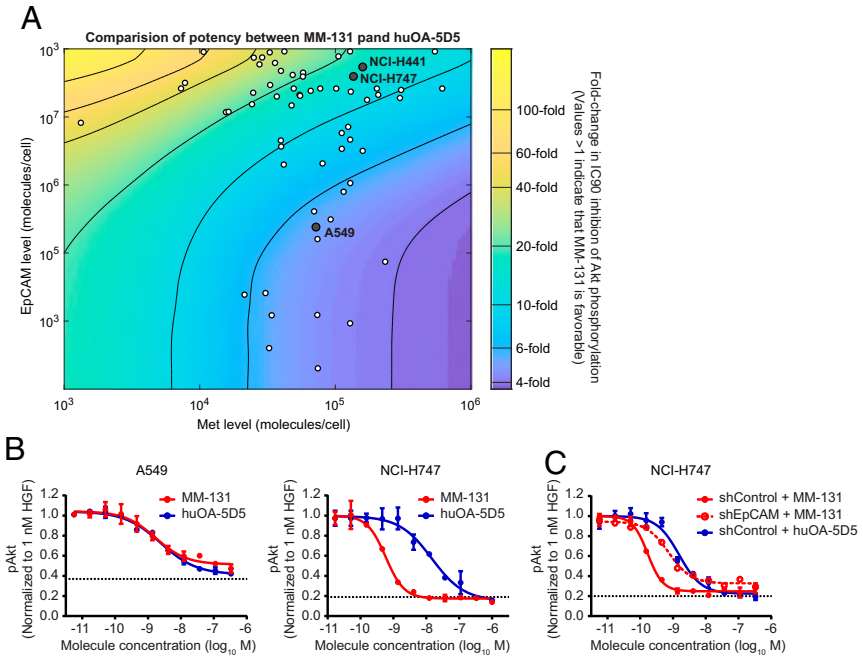

Fig. 2. EpCAM targeting increases the potency of MM-131. (*A*) Computational simulation comparing the potency of MM-131 with that of huOA-5D5. For each level of Met expression (*x* axis) and EpCAM expression (*y* axis), the IC_{90} for inhibition of Akt phosphorylation was calculated at 10 min following HGF stimulation. The values in the heat map indicate the fold change between MM-131 and huOA-5D5 (values >1 indicate that MM-131 is favorable). Dots represent a panel of cell lines with different cell surface levels of Met and EpCAM measured by quantitative fluorescence-activated cell sorting. (*B*) Testing model predictions in cell lines with low and high ratios of EpCAM/Met (0.33 for A549 and 28.9 for NCI-H747). (*C*) Testing model predictions in an isogenic cell line in which EpCAM was stably knocked down by RNAi. The EpCAM/Met ratio in NCI-H747 shEpCAM is 1.74. Antibodies were incubated with the indicated cell lines for 2 h before 10 min of stimulation with 1 nM HGF. Lysates were analyzed by pAkt ELISA; the dotted lines indicate the pAkt level in the absence of HGF and antibodies (media control). Plots in *B* and *C* reflect mean ($n = 4$) and SEM.

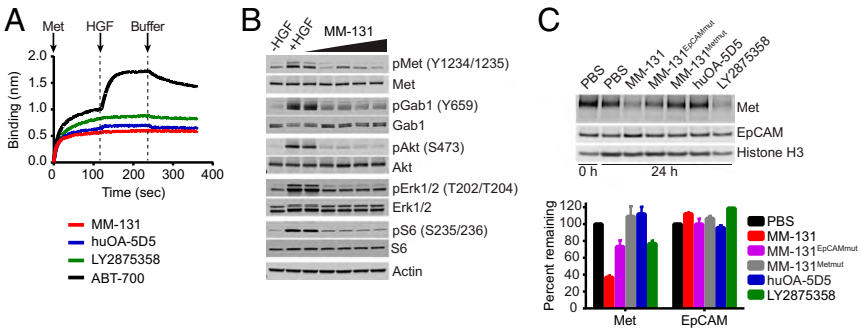

Fig. 3. MM-131 inhibits HGF-dependent and HGF-independent Met signaling by antagonizing HGF binding to Met and inducing down-regulation of Met. (*A*) MM-131 blocks HGF binding to Met. Biolayer interferometry (ForteBio) was used to measure the HGF-blocking properties of anti-Met antibodies MM-131, huOA-5D5, LY2875358, and ABT-700. Antibodies were loaded onto anti-human IgG Fc capture biosensors and incubated with 200 nM human Met. After 2 min, 200 nM human HGF was added, followed by addition of buffer at 4 min. (*B*) MM-131 inhibits HGF-induced Met signaling in a dose-dependent manner. HT-29 cells were incubated without HGF, with 1 nM HGF, or with 1 nM HGF + 0.1–1,000 nM MM-131 for 10 min and analyzed by immunoblotting with the indicated antibodies. (*C*) MM-131 down-regulates total Met levels. NCI-H2170 cells were incubated with 100 nM indicated antibodies or PBS for 24 h and analyzed by immunoblotting. Histone H3 served as a loading control. Bands were quantified using the LI-COR Odyssey imaging system. MM-131^{EpCAMmut} is a version of MM-131 with a mutation in the EpCAM scFv, preventing EpCAM binding. MM-131^{Metmut} is a version of MM-131 that cannot bind Met. Data are the mean of two independent samples; error bars indicate SD.

MM-131 that contains a mutation in CDR-H1 of the anti-EpCAM scFv that impairs EpCAM binding (MM-131^{EpCAMmut}) (Fig. 3*C* and *SI Appendix*, Fig. S6*A*). Together, the dual mechanism of action of MM-131 suggests that MM-131 will block both HGF-dependent and HGF-independent Met signaling in EpCAM-positive tumors.

MM-131 Inhibits Cancer Cell Proliferation and Migration. To determine whether the inhibition of Met signaling by MM-131 has phenotypic consequences, we examined the ability of MM-131 to inhibit cancer cell proliferation in cell lines with HGF-dependent or HGF-independent Met activation. Cell viability was assayed in 3D spheroids following 96 h of treatment with MM-131, MM-131^{EpCAMmut}, huOA-5D5, or LY2875358. As suggested by the blockade of Met signaling, MM-131 inhibits HGF-dependent proliferation of Met-positive cells (Fig. 4*A* and *SI Appendix*, Fig. S7*A*) and HGF-independent proliferation of *MET*-amplified cells (Fig. 4*B* and *SI Appendix*, Fig. S7*B*) in a dose-dependent manner. Consistent with the decrease in MM-131 potency observed in EpCAM knockdown cell lines [short hairpin EpCAM (shEpCAM); Fig. 2*C* and *SI Appendix*, Fig. S5*B*] and the incomplete down-regulation of Met by MM-131^{EpCAMmut} (Fig. 3*C* and *SI Appendix*, Fig. S6*A*), MM-131 is less effective at inhibiting proliferation in shEpCAM cells, and MM-131^{EpCAMmut} does not effectively inhibit proliferation in control cells.

Given the role of HGF/Met signaling in tumor invasion and metastasis (47), we also examined the ability of MM-131 to inhibit HGF-mediated cancer cell migration in a wound-healing assay. Cells were grown to confluence; scratched with a 96-pin wounding device; and treated with MM-131, huOA-5D5, or LY2875358 in the presence or absence of HGF. Images of the wound were captured at 2-h intervals for 24 h, and migration rates were calculated from these data. Whereas treatment with huOA-5D5 or LY2875358 allows migration and wound closure by 24 h, MM-131 inhibits HGF-mediated migration in a dose-dependent manner (Fig. 4 *C* and *E* and *SI Appendix*, Fig. S7*C*). MM-131^{EpCAMmut} slows migration and prevents wound closure but is less effective than MM-131. Notably, in the absence of HGF, huOA-5D5 and LY2875358 promote migration and wound closure, whereas MM-131 does not (Fig. 4*D* and *SI Appendix*, Fig. S7*D*). Together, these data demonstrate that MM-131 inhibits cancer cell proliferation in cell lines with HGF-dependent or HGF-independent Met activation and blocks HGF-mediated cancer cell migration. In addition, EpCAM targeting of MM-131 is critical for maximal inhibition of HGF/Met-driven proliferation and migration.

MM-131 Inhibits HGF-Dependent and HGF-Independent Tumor Growth in Vivo. To determine whether the antiproliferative activity of MM-131 observed in vitro translates to similar activity in vivo, we evaluated MM-131 in several xenograft models. As murine HGF does not activate human Met (48), we examined the activity of MM-131 in tumors with HGF-dependent Met activation by stably expressing human HGF in NCI-H358 and HCC827 lung cancer cell lines before implantation. Treatment with 12 mg/kg of MM-131 prevented growth of NCI-H358–HGF and HCC827-HGF tumors (Fig. 5*A* and *SI Appendix*, Fig. S8*A*, respectively). These results are consistent with the mechanism of action of MM-131 (Fig. 3 *A* and *C*), the inhibition of HGF-induced Met signaling by MM-131 (Fig. 3*B*), and the inhibition of HGF-mediated proliferation by MM-131 in vitro (Fig. 4*A* and *SI Appendix*, Fig. S7*A*). Notably, treatment with 10 mg/kg of huOA-5D5 or 15 mg/kg of LY2875358 (molar equivalents of 12 mg/kg of MM-131) was less effective at inhibiting tumor growth than treatment with MM-131, although the difference between MM-131 and LY2875358 was generally modest.

The antiproliferative effect of MM-131 on *MET*-amplified cells (Fig. 4*B* and *SI Appendix*, Fig. S7*B*) also translated to tumor growth inhibition in *MET*-amplified SNU-5 and MKN-45 gastric cancer and NCI-H1993 lung cancer xenograft tumors. MM-131 inhibited tumor growth more effectively than huOA-5D5 and LY2875358 in each model (Fig. 5*B* and *SI Appendix*, Fig. S8*B*). Moreover, in the SNU-5 model, a complete response was observed in 100% (seven of seven) of MM-131–treated animals, 71% (five of seven) of LY2875358-treated animals, and 0% (zero of seven) of huOA-5D5– or vehicle-treated animals (*SI Appendix*, Fig. S8*C*). Evaluation of total Met and phospho-Met levels in SNU-5 xenografts revealed significantly decreased Met and pMet levels in MM-131– and LY2875358-treated animals, whereas Met and pMet levels were unchanged following treatment with huOA-5D5 and vehicle (Fig. 5 *C* and *D*). These results are consistent with the mechanism of action of MM-131 and LY2875358 (blocking HGF binding and downregulating Met) and the inability of huOA-5D5 to down-regulate Met, and thus inhibit growth of *MET*-amplified tumors. Consistent with tumor regression in MM-131– and LY2875358-treated animals, the percentage of Ki67-positive tumor cells was lower in these tumors (Fig. 5*D*).

To determine whether EpCAM targeting of MM-131 is critical for the inhibition of tumor growth in vivo, we stably knocked down EpCAM in NCI-H441 lung and MKN-45 gastric cancer cells by RNAi (shEpCAM) and evaluated MM-131 in NCI-H441 and MKN-45 shEpCAM and shControl xenografts. Treatment

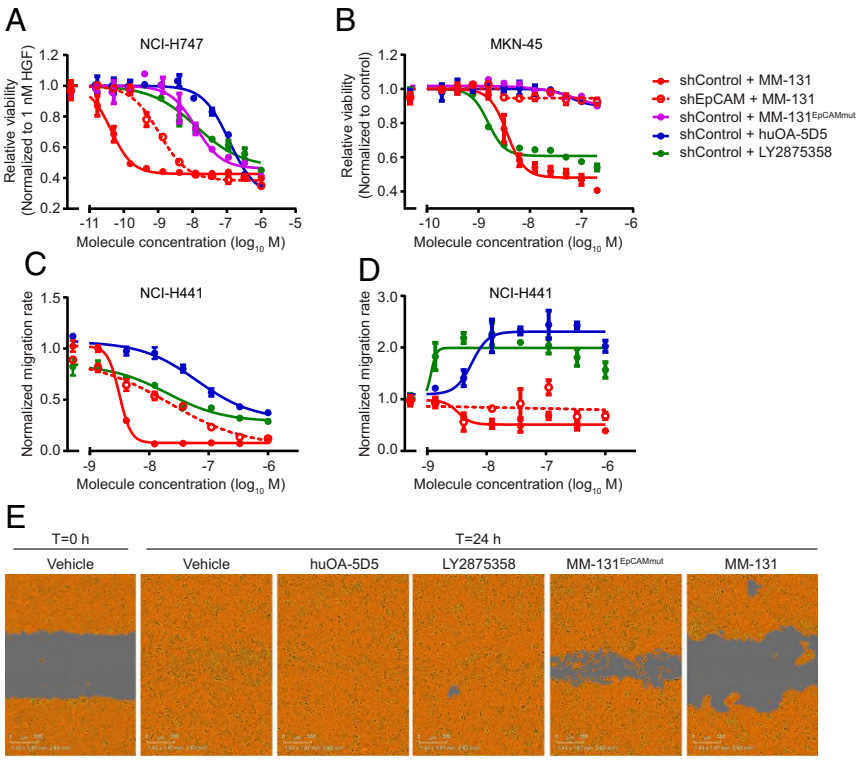

Fig. 4. MM-131 inhibits cancer cell proliferation and migration. MM-131 blocks HGF-dependent cell proliferation (*A*) and proliferation of *MET*-amplified cells (*B*) in a dose-dependent manner. NCI-H747, NCI-H441, and MKN-45 cell lines were stably transduced with lentiviral particles expressing untargeted shRNA (shControl) or shRNA targeting EpCAM (shEpCAM). Following formation of 3D spheroids, cells were treated with the indicated antibodies for 96 h. Viability was assessed by CellTiter-Glo assay and normalized to vehicle-treated cells in the presence (*A*) or absence (*B*) of 1 nM HGF. (*C*) MM-131 blocks HGF-induced cell migration in a dose-dependent manner. Following production of a uniform scratch wound, images were taken every 2 h for 24 h. Migration rates were calculated from the relative wound densities (density of cells inside the wound area/density outside the wound area) of each image and normalized to vehicle-treated cells in the presence of 1 nM HGF. (*D*) Unlike huOA-5D5 and LY2875358, MM-131 does not promote migration in the absence of HGF. A scratch wound migration assay was performed as in *C*, except in the absence of HGF. Migration rates were normalized to vehicle-treated cells in the absence of HGF. (*E*) Representative images of NCI-H441 cells from an HGF-induced migration assay. Images are from 1 μM treatment of indicated molecules. The wound area remaining is shown in gray, and the confluence mask is shown in orange. All plots reflect mean ($n = 3$) and SEM.

with MM-131 resulted in a marked reduction of tumor growth in shControl xenografts but was not effective in shEpCAM cells (*SI Appendix*, Fig. S8*D*), demonstrating that EpCAM targeting increases the activity of MM-131 in vivo. Notably, the activity of MM-131 in NCI-H441 and MKN-45 shEpCAM xenografts mirrored that of huOA-5D5, highlighting the lack of efficacy of monovalent anti-Met therapeutics in this setting and the necessity of the EpCAM-targeting arm of MM-131.

MM-131 Has No Observed Toxicity in Cynomolgus Monkeys. The Met and EpCAM epitopes recognized by MM-131 are well conserved between humans and cynomolgus monkeys (*Macaca fascicularis*). Accordingly, MM-131 binds with similar affinities to the human and cynomolgus monkey versions of both antigens (*SI Appendix*, Table S5). To determine the maximum tolerated dose of MM-131, monkeys were dosed weekly with 10 mg/kg, 30 mg/kg, or 60 mg/kg of MM-131 via i.v. infusion for 4 wk. No MM-131–related changes in clinical pathology parameters, histopathological changes, or gross pathological changes were observed at any of the dose levels. Thus, the no-observed-adverse-effect level of this study was the highest dose tested, or 60 mg/kg. Repeat dose pharmacokinetic studies in monkeys revealed a serum half-life that ranged from 12.5 to 72.4 h. Assuming MM-131 displays a longer half-life in humans than monkeys, dosing once every three half-lives could potentially support biweekly dosing in a clinical setting.

Met, EpCAM, and HGF Are Coexpressed in Tumors. Preclinical data demonstrate that MM-131 inhibits cancer cell proliferation and migration in models driven by Met signaling, and that MM-131 is most effective in cells that also express EpCAM. To determine the frequency of Met, EpCAM, and HGF coexpression in tumors, serial sections of primary tumor samples from 93 patients with colorectal cancer (CRC), 99 patients with gastric cancer, and 97 patients with non-small cell lung cancer (NSCLC) were stained for each biomarker. Expression of Met was observed in 77%, 68%, and 47% of CRC, gastric cancer, and NSCLC samples, respectively (Fig. 6). EpCAM was detected in nearly all samples (93%, 97%, and 92% in CRC, gastric cancer, and NSCLC, respectively), and coexpression of Met and EpCAM was observed in 96% of samples that scored positive for Met across all indications. Further work will be necessary to gain a more quantitative understanding of EpCAM and Met levels in both tumor samples and normal tissue. Expression of HGF in Met-positive samples was observed in 44% (81 of 185) of samples. Overall, 43% (79 of 185) of Met-positive tumors coexpressed EpCAM and HGF, suggesting a broad clinical opportunity for MM-131.

Discussion

Aberrant Met signaling plays a key role in cancer initiation, progression, metastasis, and resistance to therapy. In some cancers, Met behaves as a driver; tumors with *MET* gene amplification or mutation are often "addicted" to Met signaling for their proliferation and survival (6). *MET* amplification has been reported in ∼2% of epithelial cancers, including gastroesophageal cancers, CRC, and NSCLC, and is one of the mechanisms responsible for acquired resistance to EGFR therapy in NSCLC and CRC (12, 13, 49–52). More often, however, Met is overexpressed

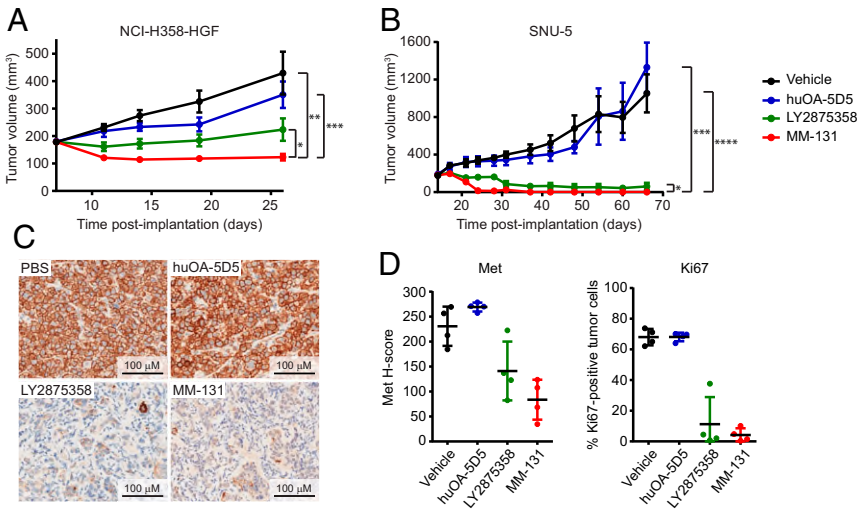

Fig. 5. MM-131 inhibits tumor growth in vivo. NCI-H358 cells expressing human HGF (NCI-H358–HGF) (*A*) or *MET*-amplified cells (SNU-5) (*B*) were implanted s.c. in athymic nude (*nu/nu*) mice. Once tumor volumes reached 100–200 mm^3, mice were randomized and dosed weekly with MM-131 (12 mg/kg), huOA-5D5 (10 mg/kg), LY2875358 (15 mg/kg), or vehicle. Tumor volume data plotted are mean ($n = 8$ in *A* and $n = 7$ in *B*) and SEM. (*A*) Final tumor volumes in MM-131–treated animals were significantly smaller than in vehicle-treated (**$P = 0.0014$), huOA-5D5–treated (***$P = 0.0003$), and LY2875358-treated (*$P = 0.0321$) groups. (*B*) In SNU-5 xenografts, final tumor volumes in MM-131–treated animals were significantly smaller than in vehicle-treated (****$P < 0.0001$), huOA-5D5–treated (***$P = 0.0001$), and LY2875358-treated (*$P = 0.0331$) treated groups. A complete response was observed in 100% (seven of seven) of MM-131–treated animals, 71% (five of seven) of LY2875358-treated animals, and 0% (zero of seven) of huOA-5D5– or vehicle-treated animals. Tumor volume data plotted are mean ($n = 7$) and SEM. (*C*) MM-131 inhibits Met activity in vivo. Representative images of pMet staining in SNU-5 tumors harvested 24 h after treatment with the indicated antibodies. (*D*) Quantification of total Met and Ki67 in SNU-5 tumors harvested 24 h after treatment with the indicated antibodies. Scatter plots show all tumors ($n = 4$ per treatment) and SD.

via transcriptional up-regulation during tumor progression by microenvironmental factors such as hypoxia, therapeutic doses of radiation, and exposure to HGF, which itself can activate Met transcription (9, 53, 54). HGF is frequently expressed in the activated stroma of primary tumors, and its expression has been linked to increased invasiveness and dissemination of tumor cells (4). In addition, elevated levels of HGF and/or Met can confer resistance to traditional therapies. Given the role of Met in oncogene "addiction," as a prometastatic factor, and as a mediator of resistance, Met is an attractive therapeutic target in many cancers. Importantly, these roles are not mutually exclusive and can evolve during tumor progression as tumor cells interact with their microenvironment.

Optimal targeting of Met requires activity in both the HGF-independent (*MET*-amplified) and HGF-dependent settings. Early clinical development of Met TKIs, most notably tivantinib, had disappointing results (55, 56), although questions were later raised concerning the target selectivity of tivantinib (15). Although many of the early Met TKI trials were performed in unselected patient populations, secondary analyses in patients with high levels of Met [as determined by immunohistochemistry (IHC)] showed signs of increased benefit. Subsequent to the phase 3 failure of tivantinib in NSCLC (57), more recent development of Met TKIs has largely focused on patients with *MET*-amplified tumors. Although promising response rates have been observed in this setting, resistance typically emerges relatively quickly and can often be attributed to tumor microenvironment-derived HGF (21) or mutations in the tyrosine kinase domain of Met (58).

Antibody-based therapeutics offer an attractive alternative to TKIs, but the clinical development of anti-Met antibodies has had limited success. Over the past decade, several anti-Met antibody therapeutics have been studied in NSCLC (mostly in combination with EGFR TKIs) and gastric cancer, where Met is frequently activated by overexpression or gene amplification. Genentech/Roche's MetMAb/huOA-5D5 seemed promising in a randomized phase II trial of erlotinib ± onartuzumab in patients with chemorefractory NSCLC (59). Although the addition of onartuzumab to erlotinib did not increase PFS or overall survival (OS) in unselected patients, significant improvements were observed in Met-positive patients, defined as having moderate (2+) to strong (3+) staining by IHC in ≥50% of tumor cells (59). Unfortunately, this result was not repeated in a similarly designed phase 3 study (METLung), where the trial was halted early for futility (60). More recently, onartuzumab was studied in a phase 3 trial in metastatic HER2-negative, Met-positive gastroesophageal cancer in combination with mFOLFOX6 (METGastric), but enrollment was stopped early due to negative final results in a similar phase 2 study (61). As with the METLung study, patients in the METGastric study were selected based on IHC staining for Met, although, in this instance, the threshold for Met positivity was set lower (IHC: 1+, 2+, or 3+).

Eli Lilly's emibetuzumab (LY2875358), a bivalent anti-Met antibody, was also recently studied in a phase 2 trial, either as monotherapy or in combination with erlotinib in patients with

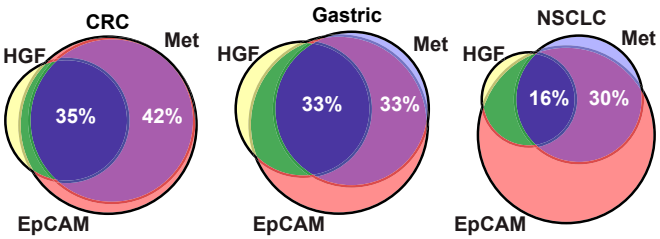

Fig. 6. Met, EpCAM, and HGF are coexpressed in tumors. Primary tumor samples were collected from patients with CRC, gastric cancer, and NSCLC. Tumors were stained for Met and EpCAM by IHC and for HGF by RNA in situ hybridization. Venn diagrams represent the percentage of tumors staining positive for Met (light blue), EpCAM (red), and HGF (yellow). Percent coexpression of Met, EpCAM, and HGF is shown in dark blue (35%, 33%, and 16% in CRC, gastric cancer, and NSCLC, respectively); percent coexpression of Met and EpCAM (in the absence of HGF) is shown in purple (42%, 33%, and 30% in CRC, gastric cancer, and NSCLC, respectively). Data used to generate Venn diagrams can be found in *SI Appendix*, Table S6.

Met-positive, metastatic NSCLC who had acquired resistance to erlotinib. In this case, Met positivity was defined as having moderate (2+) to strong (3+) staining in ≥10% of tumor cells. Unfortunately, this trial also did not meet its primary end points, which were based on objective response rates (ORRs) (62). Despite ongoing efforts, anti-Met antibody therapeutics remain unsuccessful in late-stage clinical development. Here, we submit four reasons that may underlie these outcomes:

i) Insufficient potency. Onartuzumab was designed as a monovalent antibody to prevent agonism. This reduction in valency results in decreased potency, leading to insufficient inhibition of HGF-dependent Met activation. In addition, monovalency removes the ability to down-regulate Met, rendering onartuzumab unable to inhibit ligand-independent (*MET*-amplified) tumors (Figs. 3*C*, 4*B*, and 5*B*). To circumvent this limitation, we designed MM-131 as a bispecific antibody: monovalent for Met, but also able to bind the highly expressed tumor antigen EpCAM. This strategy restores potency in the ligand-dependent setting (Figs. 1*H* and 2*B*) and restores the ability to down-regulate Met in the ligand-independent (*MET*-amplified) setting (*SI Appendix*, Fig. S6*A*). Notably, patients in both the METLung and METGastric studies were selected based on Met positivity, but those tumors that were ligand-independent, a setting in which onartuzumab has no preclinical activity (Figs. 4*B* and 5*B*), were not excluded (60, 61).

ii) Tumor-derived HGF was not considered. Although plasma HGF has been measured in several studies, HGF produced in an autocrine manner or, more commonly, by activated stroma has not been considered. This likely stems from a historical lack of qualified assays to measure tumor-derived HGF. It is unknown whether local production of HGF is critical for Met activity in the ligand-dependent setting, but it deserves attention, given the prevalence of HGF in human tumors and the predictive value it may hold (4, 11). Notably, onartuzumab is only active in the ligand-dependent setting, yet tumoral ligand levels were not reported in the phase 2 or phase 3 trials (59–61). Similarly, bivalent antibodies such as emibetuzumab (LY2875358) may agonize Met signaling in the absence of ligand, as exemplified by its promotion of migration in the absence of HGF (Fig. 4*D* and *SI Appendix*, Fig. S7*D*), yet tumoral HGF levels were also not reported in the emibetuzumab trials (62, 63).

iii) Clinical studies typically focus on inhibition of tumor growth but rarely evaluate another major role of HGF/Met signaling, that of promoting tumor cell invasion and dissemination. To date, early-stage clinical trials evaluating Met inhibitors have used the well-established surrogate end points of PFS and ORR to predict OS. The inclusion of metastasis-free survival, a measure of how long a patient remains on therapy before developing new lesions, may be a more appropriate way to evaluate a Met inhibitor in the early stages of clinical development. Additionally, trials designed specifically to evaluate prevention of metastasis in patients with premetastatic disease may also be better matched to Met biology than trials focused on patients with late-stage, metastatic disease. Notably, MM-131 inhibited HGF-mediated tumor cell migration more effectively than either huOA-5D5 or LY2875358 (Fig. 4*C* and *SI Appendix*, Fig. S7*C*) and did not promote migration in the absence of HGF, as was observed with both huOA-5D5 and LY2875358 (Fig. 4*D* and *SI Appendix*, Fig. S7*D*). It will be interesting to see if this preclinical effect on cell migration translates into an antimetastatic effect in patients.

iv) On-target toxicity. Two of the common toxicities reported in clinical trials of antibody-based Met pathway inhibitors are peripheral edema and hyperalbuminemia (64–66). Given the absence of findings suggestive of liver cell damage, as well as the role of HGF/Met in maintaining liver homeostasis (67), these toxicities likely arise from Met inhibition in hepatocytes. As hepatocytes are EpCAM-negative, the design of MM-131 may provide a wider therapeutic window in which to optimize dosing. Given the increase in potency afforded by EpCAM targeting, it is reasonable to expect that MM-131 could be dosed at a level that permits inhibition of Met in EpCAM-positive tumors cells while sparing EpCAM-negative hepatocytes. Notably, there were no gross pathological findings or changes in clinical pathology parameters in cynomolgus monkeys treated with up to 60 mg/kg of MM-131. In addition, Finisguerra et al. (68) recently reported that inhibition of Met on immune cells may negatively impact their antitumor properties, and that this may be an underlying cause of failure for some anti-Met therapies. Data from the single-cell RNA-sequencing study published by Tirosh et al. (69) indicate that they have little to no EpCAM expression, suggesting that treatment with MM-131 will not affect the antitumor immune response.

In summary, we have shown that MM-131 is a purely antagonistic anti-Met antibody that potently inhibits Met signaling in both ligand-dependent and ligand-independent EpCAM-positive tumor cells by blocking HGF binding and inducing receptor down-regulation. These mechanisms of action lead to inhibition of cancer cell proliferation and migration in vitro and inhibition of tumor growth in vivo. MM-131 has a favorable pharmacokinetic and toxicity profile and was designed to limit on-target toxicities reported for other Met inhibitors. These preclinical data support the evaluation of MM-131 in patients with *MET*-amplified, Met-overexpressed, or Met-positive/HGF-positive tumors that also express EpCAM.

Methods

Cell Lines. Cell lines were obtained from the American Type Culture Collection, National Cancer Institute Development Therapeutics Program, German Collection of Microorganisms and Cell Cultures (Leibniz Institute, Braunschweig, Germany), or Sigma–Aldrich. HCC827-GR5 cells were kindly provided by P. Jänne, Dana–Farber Cancer Institute, Boston, MA. Details can be found in *SI Appendix, Supplemental Methods*. All cell lines were maintained according to the source cell bank's recommendations or in RPMI supplemented with 10% FBS and 1% penicillin/streptomycin at 37 °C and 5% CO_2. To generate EpCAM knockdown cell lines, cells were transduced with Mission shRNA lentiviral particles against EpCAM (SHCLNV-NM_002354; Sigma–Aldrich). Mission nontarget shRNA control lentiviral particles (SHC016V) were used to generate control cell lines. To generate HGF-expressing cell lines, cells were transduced with lentiviral particles expressing human HGF (LPP-A0820-Lv105-100-S; GeneCopoeia) or control viral particles (LPP-NEG-Lv105-025; GeneCopoeia). Lentiviral transductions were carried out in the presence of 4 μg/mL polybrene, and cells were selected in 1–2 μg/mL puromycin for several weeks before use in experiments.

Expression and Purification of Antibodies. During antibody engineering, antibodies were either stably transfected into CHO-K1 cells or transiently transfected into 293F cells and harvested as described (70). Supernatants were incubated with MabSelect (GE Healthcare) while shaking at 20 °C for 1 h. Supernatant and resin were loaded onto a column (BioRad), and a vacuum was applied to separate supernatant from resin. The column was washed with a high-conductivity buffer (PBS + 0.5 M NaCl). Antibodies were eluted with 0.1 M acetic acid, neutralized with 1 M Tris buffer (pH 8.0), filter-sterilized, and dialyzed against PBS overnight at 4 °C.

MM-131 was stably expressed in a CHO-K1-GS cell line. Briefly, cells were electroporated with linearized DNA, transferred to a shaker flask, and incubated at 37 °C (120 rpm, 5% CO_2). The next day, cells were centrifuged and suspended in glutamine-free selection media containing L-methionine sulphoximine, distributed in 96-well plates at varying concentrations, and incubated at 37 °C. After 3–4 wk, the resulting minipools were screened for expression, and the top three pools were combined and adapted into Lonza proprietary media. Adapted cells were seeded into media at a density of 2×10^5 cells per milliliter, and feeds were added per manufacturer recommendations. On day 14, cells were harvested by centrifugation and the supernatant was filtered using a 0.22-μm filter.

The sequences for huOA-5D5 (29) and LY2875358 (US Patent 9201074; ref. 71) were stably expressed in CHO-K1 cells as described (70). ABT-700 (US Patent 8545839; ref. 72), MM-131^{EpCAMmut}, and MM-131^{Metmut} were transiently expressed using the Expi293 expression system (Life Technologies). Mutations were made in the paratope to eliminate binding to EpCAM and Met. On day 6, cells were harvested by centrifugation and the supernatant was filtered using a 0.22-μM filter. All proteins were purified using protein A chromatography and characterized with SEC as described (70). All antibodies were confirmed to be greater than 90% monomeric species. Final concentrations were determined using A_{280} values and theoretical extinction coefficients.

Affinity Measurements. All reagents were equilibrated, and samples were brought to room temperature before the biolayer interferometry assay (ForteBio). Streptavidin biosensors were hydrated for 10 min in protein-free blocking buffer (Pierce), followed by 10 min in PBS. Assays were run using the Octet software and procedure per the manufacturer's instructions. The assay consisted of the following steps: 10-min equilibration, 2-min biotinylated antibody loading (10 μg/mL), 1-min baseline stabilization, and 3-min incubation with the antigen listed (200–12.5 nM), followed by 5-min measurement of the dissociation. PBS was used as the matrix throughout. Data were analyzed and processed with Octet data analysis software to determine kinetic parameters [K_d, on-rate constant (k_{on}), and off-rate constant (k_{off})].

Met and EpCAM Cell Surface Quantification by Quantitative Fluorescence-Activated Cell Sorting. Cells were seeded at least 48 h before harvest. Cells were detached with Accutase (A1110501; ThermoFisher Scientific), washed, and stained with fluorescently labeled anti-Met (ABT-700) or anti-EpCAM (EBA-1; BD Biosciences) antibodies. Quantum Simply Cellular anti-human IgG beads (Bangs Laboratories) were similarly labeled. Labeled beads and cells were analyzed by flow cytometry. Four populations of beads with varying antibody-binding capacities were used as standards to quantify the number of surface receptors per cell.

ELISAs. Cell-based ELISAs were performed using standard techniques. Detailed protocols are provided in *SI Appendix, Supplemental Methods*.

HGF-Binding Assay. Biolayer interferometry (ForteBio) was used to measure the HGF-blocking properties of anti-Met antibodies. Antibodies were loaded onto anti-human IgG Fc capture biosensors and incubated with 200 nM human Met. After 2 min, 200 nM human HGF was added, followed by addition of PBS after another 2 min.

MM-131 Structure Determination. Methods for crystallization, data collection, and structure determination of MM-131 are described in *SI Appendix, Supplemental Methods* (73–75).

Degradation/Signaling Assays and Immunoblotting. For degradation assays, cells were starved overnight in media containing 0.5% FBS, incubated with 100 nM indicated antibodies or PBS for 24 h, lysed in radioimmunoprecipitation assay buffer (89901; ThermoFisher Scientific) supplemented with protease and phosphatase inhibitors as above, and analyzed by immunoblotting. For signaling assays, cells were starved overnight in media containing 0.5% FBS, incubated with 1 nM HGF and/or MM-131 as indicated, and lysed and analyzed as above. Antibodies to pMet (Y1234/35), Met, pAkt (S473), Akt, pGab1 (Y659), Gab1, pErk1/2, Erk1/2, EpCAM, actin, and histone H3 were from Cell Signaling Technology. Bands were quantitated using a LI-COR Odyssey imaging system.

Cell Proliferation Assays. To perform cell proliferation assays in 3D spheroid cultures, cells were plated into 96-well, low-binding, multispheroid culture plates (NCP-LH96-10; Scivax Life Sciences) at densities between 3,000 and 5,000 cells per well in growth medium supplemented with 4% FBS. Following 48 h of incubation to allow for spheroid formation, cells were treated with 1 nM HGF and/or antibodies, as indicated. Treatment medium was replenished after 48 h. Following 96 h of treatment, cell viability was determined by incubation with CellTiter-Glo (Promega) for 10 min, followed by luminescent readout on an EnVision plate reader (PerkinElmer). Values were normalized to vehicle-treated cells in the presence or absence of 1 nM HGF (as indicated), and dose–response curves were determined by a four-parameter fit using GraphPad Prism software.

Cell Migration Assays. Cells were grown to confluence on 96-well ImageLock plates (Essen Bioscience) and wounded with a 96-pin wound-making tool (WoundMaker; Essen Bioscience). Detached cells were removed by a serum-free medium wash. Serum-free medium containing 1 nM HGF and/or antibodies was added to wells and wounds were imaged for 24 h with the IncuCyte ZOOM live cell imager (Essen Bioscience). The relative wound density (density of cells inside relative to outside the wound) was quantified at 2-h intervals, and migration rates were calculated from these data. Values were normalized to those of cells in the absence of antibodies and treated with or without 1 nM HGF. Dose–response curves were determined by a four-parameter fit using GraphPad Prism software.

Tumor Xenografts. NCI-H358–HGF, HCC827-HGF, SNU-5, MKN-45, and NCI-H441 cells were implanted s.c. into the flank of female athymic nude (*nu/nu*) mice. NCI-H1993 cells were implanted into female BALB/c nude mice. For MKN-45 xenografts, 2×10^6 cells were implanted; 5×10^6 cells were implanted for all other models. Tumor volumes [$V = (\pi/6) \times L \times W^2$] were measured with calipers. When volumes reached 100–200 mm^3, animals were randomized according to tumor volume and body weight. Animals were dosed weekly with MM-131 (12 mg/kg), huOA-5D5 (10 mg/kg), or LY2875358 (15 mg/kg) (all equimolar equivalents), or with PBS via i.p. administration. All animal studies were conducted in accordance with the *Guide for the Care and Use of Laboratory Animals* (76). The Institutional Animal Care and Use Committee at Merrimack Pharmaceuticals reviewed and approved all animal protocols.

IHC and RNA in-Situ Hybridization. Methods for IHC and RNA in situ hybridization are described in *SI Appendix, Supplemental Methods*.

Mechanistic Computational Model. A mechanistic computational model was constructed to assess differential activities of the Met- and EpCAM-binding capabilities of MM-131 and Met binding of huOA-5D5 on pMet and pAkt signaling and their dependency on Met and EpCAM expression of the cell lines. The topology of the model includes antibody–receptor interactions, ligand-induced formation of phosphorylated dimers, and signaling to key downstream proteins. Values of the kinetic parameters in the model were constrained by fitting the model simulation to experimental dose–response and time-course data, for a technical description of the approach (77). The reactions in the model are represented as a system of ordinary differential equations. Model construction and simulation were performed with MATLAB (MathWorks) and the D2D modeling framework (http://www.data2dynamics.org/). The model topology is described in *SI Appendix*, Tables S7 and S8. All experimental data and code used for model construction and parameter calibration are available at http://www.data2dynamics.org/.

ACKNOWLEDGMENTS. We thank Victoria Rimkunas for assistance with IHC staining and scoring, Johanna Lahdenranta for assistance with HALO software analysis, Ken Olivier for design and analysis of the toxicology and toxicokinetic studies, and Jae Kim for assistance with pharmacokinetic analysis and modeling.

1. Trusolino L, Bertotti A, Comoglio PM (2010) MET signalling: Principles and functions in development, organ regeneration and cancer. *Nat Rev Mol Cell Biol* 11:834–848.
2. Gherardi E, Birchmeier W, Birchmeier C, Vande Woude G (2012) Targeting MET in cancer: Rationale and progress. *Nat Rev Cancer* 12:89–103.
3. Ferracini R, et al. (1995) The Met/HGF receptor is over-expressed in human osteosarcomas and is activated by either a paracrine or an autocrine circuit. *Oncogene* 10: 739–749.
4. Matsumoto K, Nakamura T (2006) Hepatocyte growth factor and the Met system as a mediator of tumor-stromal interactions. *Int J Cancer* 119:477–483.
5. Grugan KD, et al. (2010) Fibroblast-secreted hepatocyte growth factor plays a functional role in esophageal squamous cell carcinoma invasion. *Proc Natl Acad Sci USA* 107:11026–11031.
6. Comoglio PM, Giordano S, Trusolino L (2008) Drug development of MET inhibitors: Targeting oncogene addiction and expedience. *Nat Rev Drug Discov* 7:504–516.
7. Organ SL, Tsao M-S (2011) An overview of the c-MET signaling pathway. *Ther Adv Med Oncol* 3(Suppl 1):S7–S19.
8. Raghav KPS, Gonzalez-Angulo AM, Blumenschein GR, Jr (2012) Role of HGF/MET axis in resistance of lung cancer to contemporary management. *Transl Lung Cancer Res* 1:179–193.
9. De Bacco F, et al. (2011) Induction of MET by ionizing radiation and its role in radioresistance and invasive growth of cancer. *J Natl Cancer Inst* 103:645–661.
10. Engelman JA, et al. (2007) MET amplification leads to gefitinib resistance in lung cancer by activating ERBB3 signaling. *Science* 316:1039–1043.
11. Siegfried JM, et al. (1998) The clinical significance of hepatocyte growth factor for non-small cell lung cancer. *Ann Thorac Surg* 66:1915–1918.
12. Nakajima M, et al. (1999) The prognostic significance of amplification and overexpression of c-met and c-erb B-2 in human gastric carcinomas. *Cancer* 85:1894–1902.
13. Zeng Z-S, et al. (2008) c-Met gene amplification is associated with advanced stage colorectal cancer and liver metastases. *Cancer Lett* 265:258–269.

14. Go H, et al. (2010) High MET gene copy number leads to shorter survival in patients with non-small cell lung cancer. *J Thorac Oncol* 5:305–313.
15. Katayama R, et al. (2013) Cytotoxic activity of tivantinib (ARQ 197) is not due solely to c-MET inhibition. *Cancer Res* 73:3087–3096.
16. Gan HK, et al. (2015) cMet: Results in papillary renal cell carcinoma of a phase I study of AZD6094/volitinib leading to a phase 2 clinical trial with AZD6094/volitinib in patients with advanced papillary renal cell cancer (PRCC). *J Clin Oncol* 33(Suppl 7):487 (abstr).
17. Soo R, et al. (2015) Highly selective c-Met inhibitor tepotinib plus gefitinib is active in Asian patients with c-Met+ NSCLC. *Ann Oncol* 26:125–147.
18. Bauer TM, et al. (2016) Phase (Ph) I study of the safety and efficacy of the cMET inhibitor capmatinib (INC280) in patients (pts) with advanced cMET+ non-small cell lung cancer (NSCLC). *J Thorac Oncol* 11(Suppl):S257–S258.
19. Lennerz JK, et al. (2011) MET amplification identifies a small and aggressive subgroup of esophagogastric adenocarcinoma with evidence of responsiveness to crizotinib. *J Clin Oncol* 29:4803–4810.
20. Vassal G, et al. (2015) Activity of crizotinib in relapsed MET amplified malignancies: Results of the French AcSé Program. *J Clin Oncol* 33(Suppl 15):2595 (abstr).
21. Pennacchietti S, et al. (2014) Microenvironment-derived HGF overcomes genetically determined sensitivity to anti-MET drugs. *Cancer Res* 74:6598–6609.
22. Prat M, Crepaldi T, Pennacchietti S, Bussolino F, Comoglio PM (1998) Agonistic monoclonal antibodies against the Met receptor dissect the biological responses to HGF. *J Cell Sci* 111:237–247.
23. Pacchiana G, et al. (2010) Monovalency unleashes the full therapeutic potential of the DN-30 anti-Met antibody. *J Biol Chem* 285:36149–36157.
24. Moores SL, et al. (2016) A novel bispecific antibody targeting EGFR and cMet is effective against EGFR inhibitor-resistant lung tumors. *Cancer Res* 76:3942–3953.
25. Choi H-J, Kim Y-J, Lee S, Kim Y-S (2013) A heterodimeric Fc-based bispecific antibody simultaneously targeting VEGFR-2 and Met exhibits potent antitumor activity. *Mol Cancer Ther* 12:2748–2759.
26. Herlyn M, Steplewski Z, Herlyn D, Koprowski H (1979) Colorectal carcinoma-specific antigen: Detection by means of monoclonal antibodies. *Proc Natl Acad Sci USA* 76: 1438–1442.
27. van der Gun BTF, et al. (2010) EpCAM in carcinogenesis: The good, the bad or the ugly. *Carcinogenesis* 31:1913–1921.
28. Schnell U, Cirulli V, Giepmans BNG (2013) EpCAM: Structure and function in health and disease. *Biochim Biophys Acta* 1828:1989–2001.
29. Merchant M, et al. (2013) Monovalent antibody design and mechanism of action of onartuzumab, a MET antagonist with anti-tumor activity as a therapeutic agent. *Proc Natl Acad Sci USA* 110:E2987–E2996.
30. Harms BD, Kearns JD, Iadevaia S, Lugovskoy AA (2014) Understanding the role of cross-arm binding efficiency in the activity of monoclonal and multispecific therapeutic antibodies. *Methods* 65:95–104.
31. Ridgway JB, Presta LG, Carter P (1996) 'Knobs-into-holes' engineering of antibody CH3 domains for heavy chain heterodimerization. *Protein Eng* 9:617–621.
32. Oganesyan V, Gao C, Shirinian L, Wu H, Dall'Acqua WF (2008) Structural characterization of a human Fc fragment engineered for lack of effector functions. *Acta Crystallogr D Biol Crystallogr* 64:700–704.
33. Zhang Y, Skolnick J (2005) TM-align: A protein structure alignment algorithm based on the TM-score. *Nucleic Acids Res* 33:2302–2309.
34. Davies AM, Jefferis R, Sutton BJ (2014) Crystal structure of deglycosylated human IgG4-Fc. *Mol Immunol* 62:46–53.
35. Davies AM, et al. (2014) Structural determinants of unique properties of human IgG4-Fc. *J Mol Biol* 426:630–644.
36. Elliott JM, et al. (2014) Antiparallel conformation of knob and hole aglycosylated half-antibody homodimers is mediated by a CH2-CH3 hydrophobic interaction. *J Mol Biol* 426:1947–1957.
37. Wyrzucki A, et al. (2014) Alternative recognition of the conserved stem epitope in influenza A virus hemagglutinin by a VH3-30-encoded heterosubtypic antibody. *J Virol* 88:7083–7092.
38. Landgraf KE, et al. (2014) An allosteric switch for pro-HGF/Met signaling using zymogen activator peptides. *Nat Chem Biol* 10:567–573.
39. Krissinel E, Henrick K (2007) Inference of macromolecular assemblies from crystalline state. *J Mol Biol* 372:774–797.
40. Liu L, et al. (2014) LY2875358, a neutralizing and internalizing anti-MET bivalent antibody, inhibits HGF-dependent and HGF-independent MET activation and tumor growth. *Clin Cancer Res* 20:6059–6070.
41. Stamos J, Lazarus RA, Yao X, Kirchhofer D, Wiesmann C (2004) Crystal structure of the HGF beta-chain in complex with the Sema domain of the Met receptor. *EMBO J* 23: 2325–2335.
42. Roovers RC, et al. (1998) High-affinity recombinant phage antibodies to the pancarcinoma marker epithelial glycoprotein-2 for tumour targeting. *Br J Cancer* 78: 1407–1416.
43. Willuda J, et al. (1999) High thermal stability is essential for tumor targeting of antibody fragments: Engineering of a humanized anti-epithelial glycoprotein-2 (epithelial cell adhesion molecule) single-chain Fv fragment. *Cancer Res* 59:5758–5767.
44. Pavšič M, Gunčar G, Djinović-Carugo K, Lenarčič B (2014) Crystal structure and its bearing towards an understanding of key biological functions of EpCAM. *Nat Commun* 5:4764.
45. Münz M, et al. (2010) Side-by-side analysis of five clinically tested anti-EpCAM monoclonal antibodies. *Cancer Cell Int* 10:44.
46. Wang J, et al. (2016) Anti-c-Met monoclonal antibody ABT-700 breaks oncogene addiction in tumors with MET amplification. *BMC Cancer* 16:105.
47. Birchmeier C, Birchmeier W, Gherardi E, Vande Woude GF (2003) Met, metastasis, motility and more. *Nat Rev Mol Cell Biol* 4:915–925.
48. Rong S, et al. (1992) Tumorigenicity of the met proto-oncogene and the gene for hepatocyte growth factor. *Mol Cell Biol* 12:5152–5158.
49. Miller CT, et al. (2006) Genomic amplification of MET with boundaries within fragile site FRA7G and upregulation of MET pathways in esophageal adenocarcinoma. *Oncogene* 25:409–418.
50. Bean J, et al. (2007) MET amplification occurs with or without T790M mutations in EGFR mutant lung tumors with acquired resistance to gefitinib or erlotinib. *Proc Natl Acad Sci USA* 104:20932–20937.
51. Bardelli A, et al. (2013) Amplification of the MET receptor drives resistance to anti-EGFR therapies in colorectal cancer. *Cancer Discov* 3:658–673.
52. Turke AB, et al. (2010) Preexistence and clonal selection of MET amplification in EGFR mutant NSCLC. *Cancer Cell* 17:77–88.
53. Pennacchietti S, et al. (2003) Hypoxia promotes invasive growth by transcriptional activation of the met protooncogene. *Cancer Cell* 3:347–361.
54. Boccaccio C, Gaudino G, Gambarotta G, Galimi F, Comoglio PM (1994) Hepatocyte growth factor (HGF) receptor expression is inducible and is part of the delayed-early response to HGF. *J Biol Chem* 269:12846–12851.
55. Sequist LV, et al. (2011) Randomized phase II study of erlotinib plus tivantinib versus erlotinib plus placebo in previously treated non-small-cell lung cancer. *J Clin Oncol* 29: 3307–3315.
56. Kang Y-K, et al. (2014) A phase II trial of a selective c-Met inhibitor tivantinib (ARQ 197) monotherapy as a second- or third-line therapy in the patients with metastatic gastric cancer. *Invest New Drugs* 32:355–361.
57. Scagliotti G, et al. (2015) Phase III multinational, randomized, double-blind, placebo-controlled study of tivantinib (ARQ 197) plus erlotinib versus erlotinib alone in previously treated patients with locally advanced or metastatic nonsquamous non-small-cell lung cancer. *J Clin Oncol* 33:2667–2674.
58. Bahcall M, et al. (2016) Acquired METD1228V mutation and resistance to MET inhibition in lung cancer. *Cancer Discov* 6:1334–1341.
59. Spigel DR, et al. (2013) Randomized phase II trial of onartuzumab in combination with erlotinib in patients with advanced non-small-cell lung cancer. *J Clin Oncol* 31: 4105–4114.
60. Spigel DR, et al. (2014) Onartuzumab plus erlotinib versus erlotinib in previously treated stage IIIb or IV NSCLC: Results from the pivotal phase III randomized, multicenter, placebo-controlled METLung (OAM4971g) global trial. *J Clin Oncol* 32(Suppl 5):8000 (abstr).
61. Shah MA, et al. (2015) METGastric: A phase III study of onartuzumab plus mFOLFOX6 in patients with metastatic HER2-negative (HER2–) and MET-positive (MET+) adenocarcinoma of the stomach or gastroesophageal junction (GEC). *J Clin Oncol* 33 (Suppl):4012 (abstr).
62. Camidge DR, et al. (2016) A randomized, open-label, phase 2 study of emibetuzumab plus erlotinib (LY+E) and emibetuzumab monotherapy (LY) in patients with acquired resistance to erlotinib and MET diagnostic positive (MET Dx+) metastatic NSCLC. *J Clin Oncol* 34(Suppl):9070 (abstr).
63. Rosen LS, et al. (2017) A first-in-human phase I study of a bivalent MET antibody, emibetuzumab (LY2875358), as monotherapy and in combination with erlotinib in advanced cancer. *Clin Cancer Res* 23:1910–1919.
64. Morley R, et al. (2015) Safety of onartuzumab in patients with solid tumors: Experience to date from the onartuzumab clinical trial program. *PLoS One* 10:e0139679.
65. Strickler JH, et al. (2014) Phase 1, open-label, dose-escalation, and expansion study of ABT-700, an anti-C-met antibody, in patients (pts) with advanced solid tumors. *J Clin Oncol* 32(Suppl 5):2507 (abstr).
66. Cunningham D, et al. (2015) Phase III, randomized, double-blind, multicenter, placebo (P)-controlled trial of rilotumumab (R) plus epirubicin, cisplatin and capecitabine (ECX) as first-line therapy in patients with advanced MET-positive (pos) gastric or gastroesophageal junction (G/GEJ): RILOMET-1 study. *J Clin Oncol* 33(Suppl):4000 (abstr).
67. Huh C-G, et al. (2004) Hepatocyte growth factor/c-met signaling pathway is required for efficient liver regeneration and repair. *Proc Natl Acad Sci USA* 101:4477–4482.
68. Finisguerra V, et al. (2015) MET is required for the recruitment of anti-tumoural neutrophils. *Nature* 522:349–353.
69. Tirosh I, et al. (2016) Dissecting the multicellular ecosystem of metastatic melanoma by single-cell RNA-seq. *Science* 352:189–196.
70. Xu L, et al. (2013) Rapid optimization and prototyping for therapeutic antibody-like molecules. *MAbs* 5:237–254.
71. Davies J, Liu L, Lu J; Eli Lilly and Co. (2015) Anti-C-Met Antibodies. US Patent US 9,201,074 B2 (December 1, 2015).
72. Goetsch L, Wurch T, Bes C; Pierre Fabre Medicament (2012) Anti-C-Met Antibody. US Patent US 8,545,839 B2 (October 1, 2013).
73. Casaletto JB, et al. (2019) Heteromeric tandem IgG4/IgG1 Fc. Protein Data Bank. Available at http://www.rcsb.org/pdb/search/structidSearch.do?structureId=6HYG. Deposited October 21, 2018.
74. Casaletto JB, et al. (2019) Crystal structure of Sema domain of the Met receptor in complex with FAB. Protein Data Bank. Available at http://www.rcsb.org/pdb/search/structidSearch.do?structureId=6I04. Deposited October 25, 2018.
75. Casaletto JB, et al. (2019) Crystal structure of EpCAM in complex with scFv. Protein Data Bank. Available at http://www.rcsb.org/pdb/search/structidSearch.do?structureId=6I07. Deposited October 25, 2018.
76. National Research Council (2011) *Guide for the Care and Use of Laboratory Animals* (National Academies Press, Washington, DC), 8th Ed.
77. Raue A, et al. (2015) Data2Dynamics: A modeling environment tailored to parameter estimation in dynamical systems. *Bioinformatics* 31:3558–3560.